

STUDIES OF NEA-PHOTOCATHODES

V.V. Bakin, D.V. Gorshkov, H.E. Scheibler, S.N. Kosolobov and A.S. Terekhov,
ISP SB RAS, Novosibirsk, Russia

Abstract

Domains of validity for dipole layer and heterojunction models of the (Cs,O) – activation layer for GaAs – photocathode are determined. Two – step photoelectron escape model from NEA-photocathode is proved. Dominated elastic and inelastic scattering processes, which are accompanied the photoelectron escape, are revealed.

INTRODUCTION

In the present work we studied (Cs,O) - activation procedure of p-GaAs/(Cs,O) – photocathode and identified domains of validity for the actual models for p-GaAs/(Cs,O)/vacuum interfaces with Negative Electron Affinity (NEA). To develop photoelectron escape model and to reveal dominated mechanisms of their scattering, we discuss energy distributions of photoelectrons which were measured previously at low temperatures.

EXPERIMENTEL DETAILS

Most of experiments were performed with transmission-mode p-GaAs/(Cs,O) and p-GaN/(Cs,O) photocathodes. Details of surface cleaning and activation procedures were described in [1,2]. To measure NEA – value (χ^*), the retarding field electron energy analyzer was installed within photocathode preparation chamber (PPC). Measurements of $N_e(\epsilon_{ion})$ were performed during interruption of photocathode activation, when it was transferred to the measuring position below the mesh by rotation of carousel. Measurements of electron distributions $N_e(\epsilon_{ion})$ and $N_e(\epsilon, \theta)$ at low temperatures were performed by using of self-made parallel plate photodiodes with homogeneous electric field. Parallel plate image intensifier with microchannel plate (MCP) was used for measurements of $N_e(\epsilon_{tr})$ at RT.

EXPERIMENTAL RESULTS AND DISCUSSIONS

Determination of Actual Activation Layer Models for p-GaAs / (Cs,O) – Photocathode

At the beginning of activation, when (Cs,O) – layer is thin enough, properties of p-GaAs/(Cs,O)/vacuum interface are obviously described by dipole layer model (DLM)[3], because at this stage of activation both absolute value of NEA and QE of photocathode are increasing along with activation due to the increasing of the dipole moment of the (Cs,O) – layer. Nevertheless, it was not undoubtedly demonstrated that DLM is dominated also at the point of activation, where the

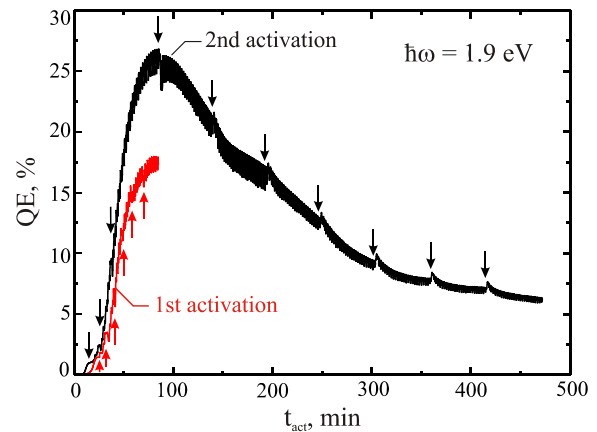


Figure 1: Time dependence of the QE during the activations.

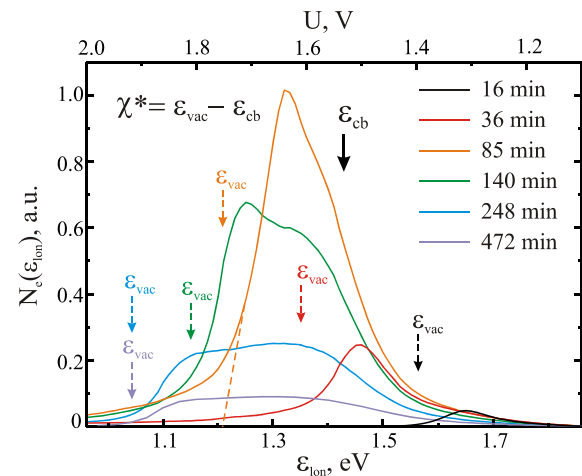


Figure 2: $N_e(\epsilon_{ion})$ – distributions measured during the 2nd activation.

absolute maximum of QE for particular photocathode occurs. To clarify this topic, we performed prolonged activation of p-GaAs/(Cs,O) – photocathode, which continued far beyond the absolute maximum of the activation curve. In addition of QE, evolution of NEA-value was monitored along with activation by periodical measurements of $N_e(\epsilon_{ion})$ – distributions. Shapes of the first (conventional) activation and the second (prolong) activations are shown on fig. 1. One can see that the second activation increase maximal QE from 18% up to 27%. One can see also, that when the absolute maximum of prolonged activation is passed, QE begins to drop down, but the rate of dropping become to be lower little by little. At the last stage of activation, at $t_{act} > 300$ min, QE drops down linearly with time. One should mention

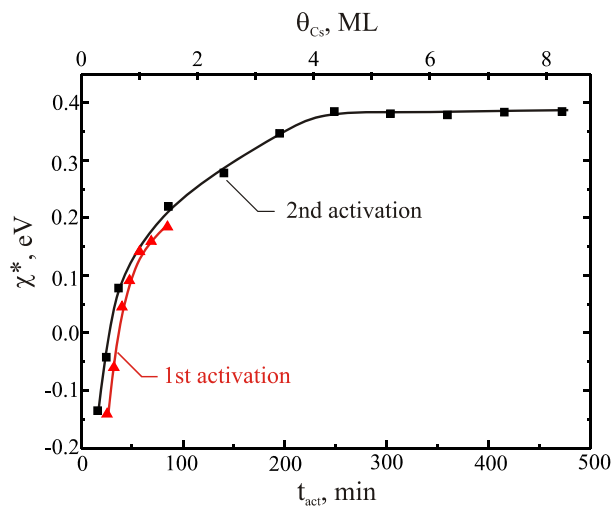


Figure 3: Time dependence of the negative electron affinity χ^* during the activations.

also, that interruptions of activation, which are marked by vertical arrows, did not “disturb” considerably the shape of the activation curve.

Fig. 2 presents part of measured $N_e(\epsilon_{\text{ion}})$ – curves, which are marked by thick arrows on fig.1. Vertical arrows on fig. 2 indicate specific energy points of $N_e(\epsilon_{\text{ion}})$ – curves. Arrow, marked by ϵ_{cb} , indicates the position of conduction band minima ϵ_{cb} in the bulk of semiconductor. It have been shown [4], that ϵ_{cb} at RT coincides with the energy, where derivative of high energy tail of $N_e(\epsilon_{\text{ion}})$ reaches its minimal value. Several dashed arrows, marked by ϵ_{vac} , indicate vacuum levels of photocathode at different points of prolonged activation. Resolution of energy analyzer within PPC was not good enough. Due to that we evaluated ϵ_{vac} by the linear approximation of the low energy tail of $N_e(\epsilon_{\text{ion}})$, as it shown on fig.2 by dashed line. The energy on this figure is counted off top of the valence band. By using of this approach, we determined ϵ_{vac} for every measured $N_e(\epsilon_{\text{ion}})$. Values of negative electron affinity (NEA) χ^* were calculated as a differences between ϵ_{cb} and ϵ_{vac} . Resulted $\chi^*(t_{\text{act}})$ - curve is shown on fig. 3. One can see, that $\chi^*(t_{\text{act}})$ grows sub-linearly during first half of prolonged activation, but thereafter saturates at its maximal value, which is close to 0.4 eV. This kind of behaviour of $\chi^*(t_{\text{act}})$ can be explained easily: during first half of activation, the (Cs,O) – layer is thin enough and due to that value of $\chi^*(t_{\text{act}})$ is dominated by the dipole moment of (Cs,O) – layer. Therefore, one can conclude that properties of p-GaAs/(Cs,O) – vacuum interface along within considerable part of the first half of activation can be described by DLM. Before the end of the first half of prolonged activation, the thickness of (Cs,O) – layer d approaches to some critical value d_{cr} , which is enough for the formation of the thin layer of solid state material with some particular band structure. Since that point, value of χ^* characterizes the band structure of this (Cs,O) – material and the constancy of χ^* during the second half of prolonged activation means, that

the band structure of this material and, consequently its composition, do not vary any more. Value of QE along the second half of activation decreases gradually with the near - linear slope. Both peculiarities of the second half of activation: constancy of χ^* and linear decreasing of QE coincide with predictions of heterojunction model (HJM) [3]. To evaluate value of d_{cr} , we did the following. At first, we took into account that the first local Cs – maximum of QE(t) during activation occurs when Cs – coverage approaches to $\theta_{\text{Cs}} \approx 0.5$ ML [5]. Secondly, we assumed that in the presence of oxygen, the sticking coefficient of Cs should be close to 1. Under this assumption value of d , which correspond to the absolute maximum of QE, was estimated to be close to 1.5 ML of Cs and the beginning of the second half of prolonged activation corresponds to $d \approx 6 - 7$ ML of Cs. Together with adsorbed oxygen, it is enough to form the band structure of thin solid state layer. Therefore, one may conclude that if thickness of (Cs,O) – layer exceeds 6-7 ML of Cs, properties of p-GaAs/(Cs,O) – vacuum interface follow predictions of HJM.

Photoelectron Escape Model

Phenomenological escape probability P_{esc} is defined as a ratio of external and internal photocurrents. External photocurrent can be measured in vacuum, while internal photocurrent should be calculated at the boundary between near-surface band bending region (BBR) and the bulk of semiconductor. To describe $N_e(\epsilon_{\text{tr}})$ and $N_e(\epsilon_{\text{ion}})$ of emitted photoelectrons from NEA – photocathode, one have to develop the microscopic description of escape process. To do that, one has to consider self-consistently the electron transport across BBR and semiconductor – vacuum interface. This description should include size quantization of electron spectra within BBR, because the width of BBR in p-GaAs with optimal concentration of charged acceptors is close to 10 nm [6]. Moreover, elastic and inelastic scattering of photoelectrons within BBR and during their escape should be included also. Bell [3] was probably the first, who put attention to the necessity of quantum description of electrons within BBR of photocathode. Mills [7] and Mills and Ibach [8] stressed, that inelastic scattering processes of low energy electrons during their escape coincide, with those, which dominated HREELS – spectra. For p-GaAs these processes consist of photoelectron interaction with Fuchs – Kliever surface optical phonons and with surface plasmons [9]. The importance of quantization of electron spectra within BBR of p-GaAs(Cs,O) - photocathode and the considerable contribution of Fuchs – Kliever surface optical phonons to the scattering of photoelectrons during their escape was revealed experimentally by measurements $N_e(\epsilon_{\text{ion}})$ – distributions at low temperatures. To detect these phenomena in p-GaAs(Cs,O) – photocathode, we studied $N_e(\epsilon_{\text{ion}})$ – distributions at $T = 4.2 - 77$ K range [6,10]. Fig. 3 reproduces $N_e(\epsilon_{\text{ion}})$ from [6], which demonstrates the quantization of electron spectra within BBR and emission of Fuchs – Kliever

surface optical phonons during photoelectron's escape. One can see on fig. 4, that $N_e(\epsilon_{ion})$ contains fine structure: the sharp peak I_0 in the vicinity of ϵ_{cb} together with weak peak I_1 and knee I_2 at lower energies. Value of ϵ_{cb} was calculated by use of energy diagram of GaAs, the known energy of exciting photons ($\hbar\omega = 1.7$ eV) and measured energy positions of two peculiarities, which were detected in the derivative of $N_e(\epsilon_{ion})$ (dot line on fig. 3). These peculiarities are related to the photoemission of ballistic photoelectrons, which are excited from the heavy holes band ($hh-c$) and from the light holes band ($lh-c$). Comparison of ϵ_{cb} and with energy position of peak I_0 led us to the conclusion that this peak is positioned 20–30 meV below ϵ_{cb} . Electrostatic potential and 2D - electron spectrum within band bending region (BBR) were calculated by the self-consistent solution of Poisson and Schrödinger equations [6] as a function of both band bending V_b and acceptor concentration N_a . It was concluded, that for the actual value of N_a and for expected values of V_b , BBR in our photocathode contains two 2-D quantum electron bands. The bottom of the upper band is positioned slightly below ϵ_{cb} , while the lower 2-D band is positioned in the vicinity of ϵ_{vac} . Therefore, it was concluded, that peak I_0 corresponds to the elastic emission of photoelectrons from the bottom of the upper 2-D quantum band. Energy intervals $\Delta_{1,2}$ between positions of peak I_1 and knee I_2 and position of peak I_0 were found to be equal to: $\Delta_1 = \hbar\Omega_x$ and $\Delta_2 = 2 \times \hbar\Omega_x$, were $\hbar\Omega_x = 38 \pm 3$ meV. Value of $\hbar\Omega_x$ coincides within experimental accuracy with the energy of Fuchs – Kliever surface optical phonons $\hbar\Omega_{FK} = 36$ meV [11], which was measured by use of high resolution electron energy loss spectroscopy (HREELS) in undoped GaAs. It was found also [12], that phonon – related losses are well pronounced in HREELS – spectrum of heavily doped p – doped GaAs. The presence of energy losses, related to Fuchs – Kliever phonons and the absence of energy losses, related to the interaction of electrons with surface plasmons, was explained in [12] by the repulsion of holes from the surface by the BBR – potential. The importance of this repulsion was confirmed in [9]. On the other side, it was demonstrated, that in the absence of band bending, electron energy losses in heavily doped p-GaAs, measured by HREELS, are dominated by the emission of surface plasmons [9]. Instead of sharp peaks of phonon-related losses [11], the shape of plasmon - related energy losses looks like a broad (but intensive!) shoulder [9,13], because surface plasmons in heavily doped p – GaAs are dumped considerably. The width of this shoulder for actual value of p is as high, as ~60 meV [9]. One should to mention also, that in p-GaAs/(Cs,O) - photocathode electron – surface plasmon scattering could be intensified because the maximum of the wave function of photoelectron at the upper quantum band within BBR of p-GaAs(Cs,O) - photocathode is located near the inner border of BBR [6]. Therefore, one can conclude, that plasmon – related energy losses of photoelectrons in p - GaAs(Cs,O) photocathodes could be considerable, but it

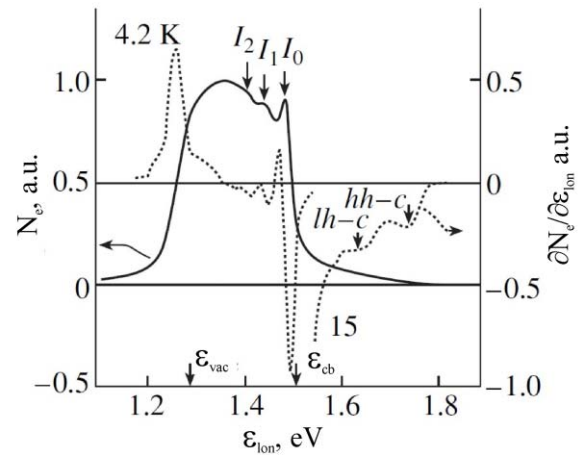


Figure 4: $N_e(\epsilon_{ion})$ – distribution measured at 4.2 K (solid line) and derivative of the $N_e(\epsilon_{ion})$ (dash line).

is not easy to reveal the intensity of these losses because they do not manifest itself by sharp structures in $N_e(\epsilon_{ion})$.

We have found, that energy intervals Δ between ϵ_{cb} and energy positions of peaks I_0 , which were measured at different photocathodes and at different temperatures 4.2 K and 77 K, are near the same. The universality of Δ means, that energy positions of upper 2-D quantum band within BBR at different photocathodes with different concentrations of acceptors, different values of χ^* , different thicknesses of the activation layers are near the same. This finding led us to conclusion, that this specific value of Δ should have some physical sense. To find out this sense, the following model is proposed. It is known, that (Cs,O) – activated surface of p-GaAs – photocathode is highly reflective [14,15] for photoelectrons with kinetic energies, which exceed ϵ_{cb} , and due to that the probability of their escape after single collision with surface does not exceed ~1%. To explain the high value of escape probability of photoelectrons with kinetic energies below ϵ_{cb} , it was assumed [6,15] that before escape photoelectrons should be trapped to the electron states within BBR. When photoelectrons are trapped, they are collided with surface repeatedly and the probability of their escape increases [15]. To realize this scenario, value of Δ should have some compromise value. On the one hand, Δ should be low enough to “simplify” fast trapping of photoelectrons to the upper 2-D quantum band, because this probability is limited by the probability of the photoelectron energy loss. The most efficient mechanism of the photoelectron energy losses near the surface is the emission of surface optical phonons. Therefore, to provide effective trapping of photoelectrons, value of Δ should not exceed the energy of surface optical phonons. On the other hand, to prevent fast thermal “re-excitation” of trapped photoelectrons to the bulk of semiconductor, value of Δ should not be too low. It seems to us that measured value of $\Delta = 20 - 30$ meV could be an appropriate compromise, which could provide the effective trapping of photoelectrons within BBR. Probability of “re-excitation” should be lower or be

compatible with probability of photoelectron escape to the vacuum and with probability of photoelectron surface recombination via defect – induced surface states with lower energies. Therefore, to provide maximal value of P_{esc} , Δ should be adjusted to the value within 20–30 meV. This adjustment is performed during activation of photocathode, when we maximize value of P_{esc} by varying both thickness and composition of (Cs,O) – layer. Our GaAs - surface cleaning procedure provides low density of charged defects at the surface and due to that, variations of parameters of (Cs,O) – layer is accompanied by the variation of V_b [16,17]. By-turn, variation of V_b causes variation of energy positions of 2-D quantum bands within BBR [6]. Therefore, during of activation of “defect-free” photocathode surface we are reaching highest P_{esc} , together with optimization of other essential parameters, Δ is also adjusted to its optimal value.

STUDY OF TRANSVERSE ENERGY DISTRIBUTIONS FROM NEA – PHOTOCATHODES

Experimental studies of energy and angular distributions of photoelectrons, emitted from NEA – photocathodes, enable one to understand better the physics of photoelectron escape. Data obtained have a practical meaning also, because they can be used for the calculation of the point spread function of position-sensitive photon detectors, for the calculation of mean transverse energy and for the calculation of the physical limit of “hallo” of electron beams. Experimental methods, which enable one to measure accurately both energy and angular distributions of photoelectrons, are well developed in for high photon energies, when kinetic energies of photoelectrons exceed 5 - 10 eV. Kinetic energies of photoelectrons, which are emitted from NEA - photocathodes are within 0.0 – 1.0 eV – interval. Due to low kinetic energies, trajectories of photoelectrons from NEA – photocathodes are extremely sensitive to the electric fields in the vicinity of photocathode, which are could vary in time due to adsorption and desorption processes. To overcome these problems we use parallel – plate photoelectron spectrometers, which are most



Figure 5: Photo of vacuum-sealed XHV - devises, which were used as a parallel-plate electron spectrometers.

suitable for measurements of $N_e(\epsilon_{lon})$ – and $N_e(\epsilon_{tr})$ – distributions. Different versions of these spectrometers operate in homogeneous electric and magnetic fields. To simplify the design of spectrometers, transmission – mode photocathodes are used. To provide homogeneity of electric field, diameters of photocathode and opposite electrode should be much more, than the distance between them. Actual homogeneities of work-functions of both electrodes can be measured. Time stability of work-functions is guaranteed by the use of XHV – conditions. We realized these spectrometers as a compact, vacuum-sealed XHV - devises, which do not contain any magnetic materials and can be cooled by direct immersion to the liquid nitrogen [10] or helium [6]. Some examples of these spectrometers are presented on fig. 5. Examples of their use are described below.

Ballistic Photoemission from p-GaAs - (Cs,O) – Photocathode

Sharp peak I_0 , which was observed in low temperature $N_e(\epsilon_{lon})$ was interpreted as a elastic escape of photoelectrons, which were concentrated within $\sim kT$ energy interval near the bottom of 2-D quantum band. The distribution of these electrons along with transverse energy or along with total energy (ϵ) and emission angle (θ), were not measured. To determine $N_e(\epsilon, \theta)$, we developed electron spectrometer, which operates in homogeneous magnetic and retarding electric fields, which are perpendicular to each other. It have been shown theoretically [18], that if to measure photocurrent J_{ph} within parallel plate photodiode as function of retarding voltage U_{ret} and magnetic field strength H , the resulted function $J_{ph}(U_{ret}, H)$ can be recalculated to $N_e(\epsilon, \theta)$ - distribution. Experiments were performed at 77K. One can see (see fig. 6), that measured $N_e(\epsilon_{lon})$ – distribution contains peak I_0 and one phonon replica. To determine angular distribution of photoelectrons within peak I_0 , the retarding voltage U_{ret}^* cut off all electrons with ϵ_{lon} , which are lower than energy, which correspond to the maximum of I_0 . Fig.7 presents $\partial J_{ph}/\partial U_{ret}(U_{ret}^*, H)$, while Fig.8 shows $N_e(\theta)$ – distribution, which was obtained from $\partial J_{ph}/\partial U_{ret}(U_{ret}^*, H)$. Details one can find in [10]. One can see on fig. 8, that $N_e(\theta)$ consist of narrow peak and broad halo. Narrow peak in the $N_e(\theta)$ – distribution contains electrons, which were escaped ballistically, without any momentum scattering. In contrary, electrons within halo were escaped along with diffusive scattering of their momentum. Our future studies should reveal the dominant mechanism of elastic diffusive momentum scattering of elastically emitted photoelectrons: is it surface roughness, disorder within (Cs,O) – layer, or the tangential component of the electric field, which occurs because of randomly distributed charged bulk acceptors and surface defects.

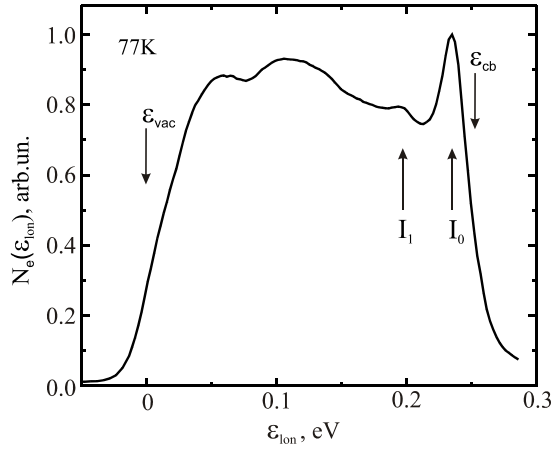
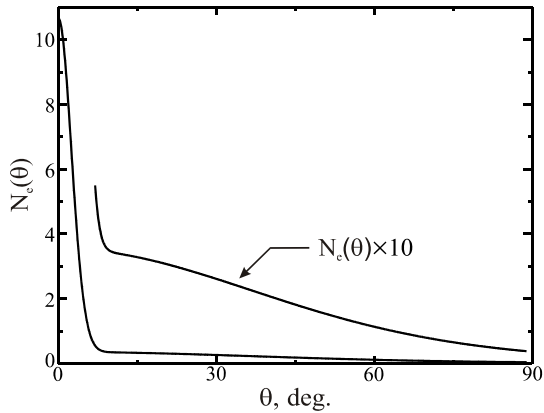
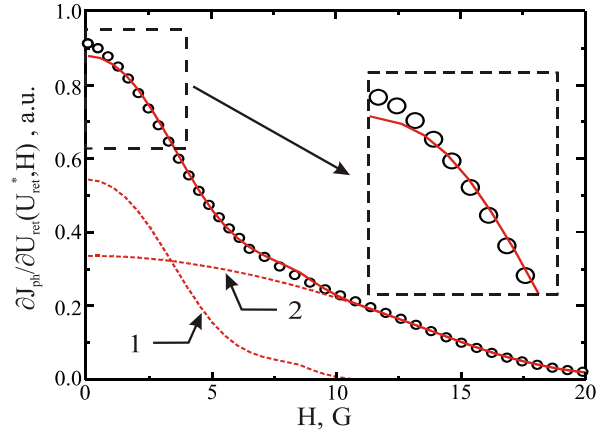
Figure 6: $N_e(\epsilon_{ion})$ – distribution measured at 77 K

Figure 8: Photoelectron angular distribution.

Transverse Energy Distribution of Photoelectrons Emitted from p-GaN(Cs) – Photocathode

To determine $N_e(\epsilon_{tr})$, the spread of electron beam in the homogeneous accelerating electric field could be measured [19]. We utilized this principle by use of homemade parallel plate image intensifier with transmission – mode p- GaN(Cs,O) – photocathode, microchannel plate and luminescent screen with 18 mm working diameters. Light spot with $\sim 25 \mu\text{m}$ FWHM - diameter and radial intensity distribution $N_{ph}^i(\rho)$ was formed at the centre of photocathode by the use of xenon arc lamp, grating monochromator with circular diaphragm at the exit slit and quartz lenses. Electrons moved within gap $d \approx 1\text{mm}$ between photocathode and MCP under the influence of accelerating voltage U_a . Simultaneously, they move along ρ in accordance with $N_e(\epsilon_{tr})$ and form broadened radial distribution of electrons $N_e(\rho)$ near MCP. After intensification by MCP, $N_e(\rho)$ was transferred to the screen. Optical replica $N_{ph}^f(\rho)$ of $N_e(\rho)$ was transferred to the digital cooled megapixel CCD-camera and then to PC. To account for the real shape of $N_{ph}^i(\rho)$ and for other

Figure 7: Measured (dots) and calculated (lines) magnetic field dependence $\partial J_{ph}/U_{ret}(U_{ret}^*, H)$.

distortions of electron and light beams within experimental setup, we expressed the measured $N_{ph}^f(\rho)$ – distributions as a multiple integral convolution. After taking into account several reasonable simplifications it was transformed to the following form:

$$N_{ph}^f(\rho) = \int N_e \left(\epsilon_{tr} = \frac{e \times U_a \times |\vec{\rho}|}{4 \times d^2} \right) \times \Psi(\vec{\rho} - \vec{\rho}_1) d\vec{\rho}_1. \quad (1)$$

were e is electron charge and $\psi(\rho)$ is the instrument function of our set up. By substituting in (1) several $N_{ph}^f(\rho)$ – distributions, which were measured at different U_a , we obtained several integral equations for two unknown functions: $\psi(\rho)$ and $N_e(\epsilon_{tr})$. Equations (1) were solved for several U_a by using standard methods from [20]. More details will be given elsewhere. Measured $N_e(\epsilon_{tr})$ – distribution is shown on fig. 9 together with $N_e(\epsilon_{ion})$ - distribution. One can see, that $N_e(\epsilon_{tr})$ contains three parts: (i) the pronounced peak at lowest ϵ_{tr} , (ii) the broad tail at “middle” energies and (iii) the high energy shoulder with near - exponential shape, which restrict the total width of $N_e(\epsilon_{tr})$. This shape was interpreted as follows. Most of electrons with lowest ϵ_{tr} has high ϵ_{ion} . Due to that “fast” photoelectrons have higher probability to “run away” from the surface without excitation of surface phonons and without scattering by random electron field in the close vicinity of photocathode surface. One should mention here, that electron scattering by surface phonons near GaN – surface is much more intensive than near GaAs – surface [21]. The energy position of the high energy shoulder is determined by the value of χ^* of p – GaN/(Cs,O) – photocathode while the near - exponential tail forms by electrons, which gained energy from surface phonons. It is seen also, that total widths of $N_e(\epsilon_{tr})$ and $N_e(\epsilon_{ion})$ are near the same, because both are limited by value of χ^* .

To evaluate the accuracy of determined $N_e(\epsilon_{tr})$ and $\psi(\rho)$, we have solved the “inverse problem” and used these

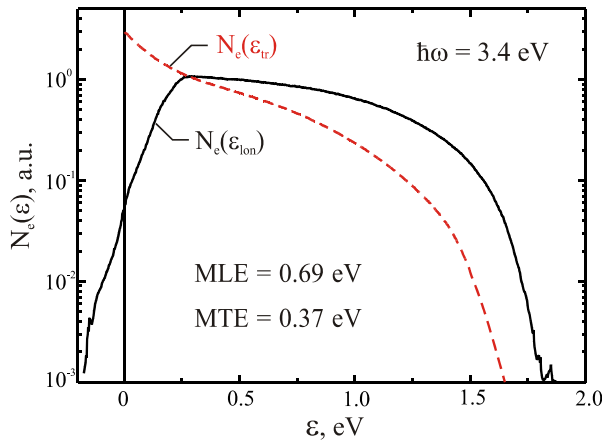


Figure 9: $N_e(\epsilon_{ph})$ – distribution (red dash line) and $N_e(\epsilon_{ion})$ – distribution (solid dark line) of electrons, emitted from p-GaN(Cs,O) -photocathode.

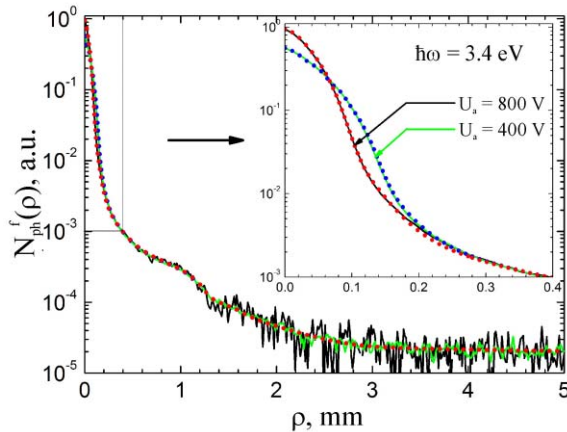


Figure 10: Measured (lines) and calculated (dots) radial intensity distributions $N_{ph}^f(\rho)$.

functions for the calculation of $N_{ph}^f(\rho)$ – distributions for different U_a . Results of these calculations, which are marked by dots on fig. 10, were compared with measured (continuous) $N_{ph}^f(\rho)$ – curves. One can see, that calculated points and measured curves coincide well.

SUMMARY AND CONCLUSIONS

The final conclusions are as follow. (i) NEA – state on p-GaAs(Cs,O) – surface can be prepared with different thicknesses of (Cs,O) – layer. Photocathodes with “thin” layers can be described by dipole layer model, while photocathodes with “thick” layers follow predictions of heterojunction model. (ii) Escape of photoelectron includes two basic steps: at the first step it is trapped by 2-D can quantum band near the surface while at the second step is escaped to the vacuum. Small part of electrons is escaped ballistically, while most of them is accompanied by various scattering processes: inelastic scattering of surface phonons and plasmons, elastic scattering by electric field of randomly distributed surface and bulk charged centres together with short range

random potential of (Cs,O) layer. (iii) To study the actual energy diagram of GaAs(Cs,O)/vacuum – interface and photoelectron escape, parallel plate electron spectrometers with energy and angular resolutions are well effective at temperatures within 4.2 K – 300 K range.

REFERENCES

- [1] O.E. Tereshchenko et al., J. Vac. Sci. Technol. A 17 (1999) 2655.
- [2] V.V. Bakin et al., e-J. Surf. Sci. Nanotech. 5 (2007) 80.
- [3] R.L. Bell, *Negative electron affinity devices*, (Oxford: Clarendon Press, 1973) 148.
- [4] A.S. Terekhov, D.A. Orlov, JETP Letters 59 (1994) 864.
- [5] O.E. Tereshchenko et al, JETP Letters 79 (2004) 163.
- [6] D.A. Orlov et al, JETP Letters 71 (2000) 220.
- [7] D.L. Mills, Surf. Sci. 48 (1975) 59.
- [8] H. Ibach, D.L. Mills, *Electron energy loss spectroscopy and surface vibrations*, (Academic Press, 1982) 336.
- [9] Y. Meng et al. Phys. Rev. B 44 (1991) 4040.
- [10] V.V. Bakin et al, JETP Letters 77 (2003) 167.
- [11] A. Degiovanni et. al, Surf.Sci. 251/252 (1991) 238.
- [12] R.G. Egdell et al, J. Electron Spectrosc. Related Phen. 45 (1987) 177.
- [13] Y. Meng et al. Phys. Rev. B 45 (1992) 1500.
- [14] A.L. Musatov et. al, Izv. Akad.Nauk SSSR, Ser. Fiz 40 (1976) 2523 (in Russian).
- [15] A.L. Musatov et. al, Izv. Akad.Nauk SSSR, Ser. Fiz 46 (1982) 1357 (in Russian).
- [16] V.L. Alperovich et al., Phys. Rev. B 50 (1994) 5480.
- [17] V.L. Alperovich et al., Appl. Phys. Lett. 66 (1995) 2122.
- [18] V.E. Andreev, A.L. Bukhgeim, A.S. Terekhov, Journal of Inversed and Ill-Posed problems, 7 (1999) 427.
- [19] G. Vergara et.al., J. Appl. Phys., 80 (1996) 1809.
- [20] R.C. Gonsalez, R.E. Woods, *Digital Image Processing, 2nd Edition*, (Prentice Hall, 2002) 780.
- [21] S.P. Grabowski et.al., Appl. Surf. Sci., 123/124 (1998) 33.